

Recent Electroweak Results from SLC/SLD¹

Raymond E. Frey

representing the SLD Collaboration

Physics Department, University of Oregon²

Eugene, Oregon 97403

E-mail: rayfrey@bovine.uoregon.edu

Abstract

Key electroweak measurements performed by the SLD collaboration at the SLC are described and recent results given. The left-right cross-section asymmetry, A_{LR} , has been updated to include the 1996 data. It remains the single most precise measurement of $\sin^2 \theta_W^{\text{eff}}$ and it is compared to the LEP results. The polarized differential cross section for b -quarks is measured and is used to perform a unique direct measurement of the parity violation parameter for b quarks, A_b . The excellent capability to perform secondary vertexing at SLC with CCD-based vertex detectors is described, including first physics results with the new detector VXD3. The vertexing is used to full advantage to make a highly pure B tag to measure the fraction of hadronic Z^0 decays going to b quarks, R_b . The vertexing, in combination with electron-beam polarization, is used to measure B_d^0 mixing. The prospects for making a B_s^0 mixing measurement are excellent given good SLC performance in the upcoming SLC run(s).

1. Introduction

Two key elements of Z^0 physics measurement at the SLAC Linear Collider (SLC) have made possible a set of unique precision electroweak tests of the Standard Model (SM). Highly longitudinally polarized electron beams directly probe the parity-violating nature of electroweak physics, greatly enhancing the measurement of key parameters such as A_e and A_b . In addition, the inherent interaction point properties of linear e^+e^- colliders, namely a tiny and very stable interaction region and a low collision rate, have allowed the SLD experiment to push the technique of precision vertexing to a new level. These assets have enabled SLD to make a set of SM tests at comparable precision to those of LEP, while using largely independent measurement techniques.

¹ Presented at *Beyond the Standard Model V, Balholm, Norway, April 29 – May 4, 1997.*

²Supported by DoE award DE-FG03-96ER40969.

Polarized Beam

The production and transport of longitudinally polarized electron beams at SLC has been discussed in detail elsewhere[1]. Polarized electrons are photoproduced from a strained GaAs cathode by means of circularly polarized laser light with $\lambda \approx 850$ nm. The sign of the laser polarization is controlled such that it follows a pseudo-random pulse-by-pulse sequence. Before the electron beam enters its damping ring, the polarization is rotated into the vertical by means of a 6.34 T-m solenoidal field. As it turns out, the wavelength of betatron oscillations of the collider arc is very nearly equal to the distance for electron spin-precession. Hence, spin precession in a non-bend plane can accumulate during the normal arc focussing-defocussing beam transport. This allows the vertical polarization at the end of the linac to become longitudinal at the collision point by means of the beam “launch” in position and angle at the entrance to the arc. The launch can be carefully tuned at the same time that polarization measurements at SLD are made. A thorough optimization is carried out in this way during initial running setup, and is subsequently checked and re-optimized periodically during the run. Occasionally, changes of beam orbit in the arc due to normal accelerator tuning lead to small changes in polarization ($\sim 0.5\%$) with timescales of hours. Meanwhile, polarization measurements are performed every 3 minutes during normal data taking, with each measurement having statistical resolution of $\approx 0.5\%$. Hence, any modulations in polarization are recorded and applied to the corresponding (in time) Z^0 events. A summary of the polarization measurement and systematic effects is given below in the A_{LR} section.

The electron and positron beams at SLC are each focussed at the collision point to a typical size of $(\sigma_x, \sigma_y, \sigma_z) = (2.1, 0.6, 500)\mu\text{m}$. This allows for a small-diameter beampipe and vertex detectors which can be placed close to the collision point, thus reducing extrapolation error. Equally important is the fact that the collision point is very stable. Its transverse movement is usually less than a few microns between measurements of the position, which requires a few tens of Z^0 events. The resulting accuracy for determining the interaction point position is $\approx 7 \mu\text{m}$ in x and y , and $\approx 40 \mu\text{m}$ in z . Not only does this significantly improve the precision for measuring decay lengths or impact parameters, it also means that particles which decay after short flight paths can be separated from the primary interaction point. Besides improving the efficiency for tagging b -quark and c -quark flavored hadrons and τ leptons, the Z^0 decay modes involving these final states can be vetoed to allow studies of enhanced samples of Z^0 decays to u and d quarks. The latter principle of light-flavor tagging has been used at SLD for QCD measurements, but is not discussed further here. The low 120 Hz collision rate at SLC opens a window of opportunity for exploiting an intrinsic 3-D pixel technology for the vertex detector. In particular, CCD-based detectors have been developed and utilized for SLD, starting with VXD2 in 1992.

VXD3: The Vertex Detector Upgrade

Full realization of the physics potential of the CCD-based VXD2 vertex detector was achieved after a few years of experience. It soon became clear that an improved detector, exploiting the rapid improvement in commercially available CCDs, could be made. The

most obvious characteristic of the upgrade to VXD3 can be seen in Fig. 1, namely the expanded coverage both transversely and longitudinally. This was made feasible because it had become possible to fabricate individual CCDs of much larger size. The transverse geometry was improved in two major aspects: The layout of the CCD ladders was configured such that all tracks would have three good hits, one in each of the three layers. Secondly, the expanded distance between layers provides an improved resolution for track extrapolation inward to the collision point and outward to match the tracks found in the central drift chamber. From the righthand diagram of Fig. 1 it is clear that VXD3 also extends the coverage in $\cos\theta$ significantly, with the 3-hit and 2-hit vertexing capability extending to $|\cos\theta|$ of 0.85 and 0.90, respectively. This is a substantial improvement relative to VXD2 and has important physics implications, particularly with regard to the polarized forward-backward b -quark asymmetry. The large forward-backward asymmetry for b vs \bar{b} with polarized beam means that the forward coverage is very important not only for the measurement of A_b , but also as an initial-state tag for B^0 mixing measurements. This is discussed later.

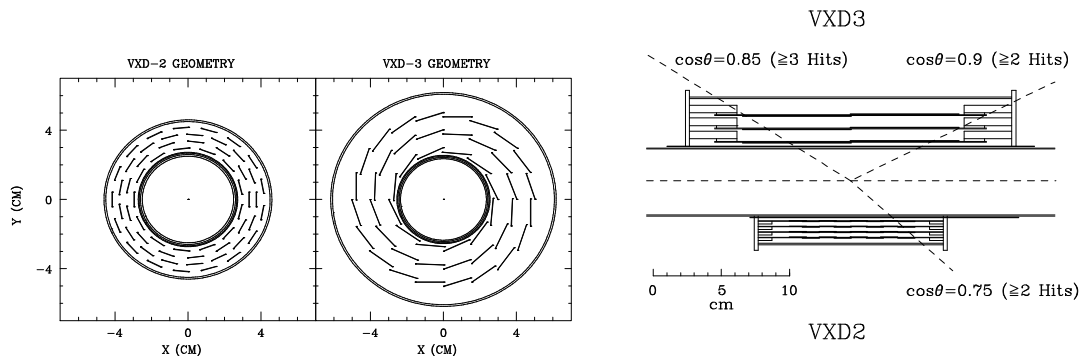


Figure 1: Geometry of VXD3 upgrade, x - y view (left) and r - z view (right).

Table 1: Comparison of VXD2 and VXD3 parameters. σ_b is impact parameter resolution with p in GeV/ c .

Parameter	VXD2 (1992–95)	VXD3 (1996– ?)
# CCDs	480	96
# pixels	1.1×10^8	3.1×10^8
Rad. Lengths	4.1%	2.1%
$\sigma_b(xy)$ (μm)	$11 \oplus 70/p$	$9 \oplus 29/p$
$\sigma_b(rz)$ (μm)	$38 \oplus 70/p$	$14 \oplus 29/p$

Table 1. summarizes a few key parameters of the upgrade of VXD2 to VXD3. Most of the SLD data has been recorded with VXD2. However, we present here preliminary results for the 1996 run with VXD3. The improvements in coverage and resolution

have a clear impact, as the b and c -quark measurement errors for the 1996 data, while representing only about 25% of the data, are in many cases comparable to those of the VXD2 period.

SLD also has a powerful particle identification system which has made a noticeable impact on the electroweak physics. This Cherenkov Ring Imaging Detector (CRID) is similar in concept to the system used by DELPHI at LEP, and the results are of similar quality. Its use for electroweak physics has been to tag K^\pm , and hence identify b vs \bar{b} via the $b \rightarrow c \rightarrow s$ cascade. Charged particle momentum measurement is made by the central drift chamber which is emersed in a uniform 0.6 T solenoidal field. Electron identification and total energy measurement is performed by a finely-segmented liquid-argon calorimeter (LAC) which provides complete coverage for $|\cos\theta| < 0.98$. Muon identification and magnetic field return takes place in the “warm” iron calorimeter (WIC).

2. The Left-Right Cross-Section Asymmetry

The left-right cross-section asymmetry is defined as

$$A_{LR} \equiv (\sigma_L - \sigma_R) / (\sigma_L + \sigma_R), \quad (1)$$

where σ_L and σ_R are the e^+e^- production cross sections for Z bosons with left-handed and right-handed electrons, respectively. To leading order, the Standard Model predicts that this quantity depends upon the vector (v_e) and axial-vector (a_e) couplings of the Z boson to the electron current,

$$A_{LR} = A_e = \frac{2v_e a_e}{v_e^2 + a_e^2} = \frac{2 [1 - 4 \sin^2 \theta_W^{\text{eff}}]}{1 + [1 - 4 \sin^2 \theta_W^{\text{eff}}]^2} \quad (2)$$

We retain the tree-level relations between the couplings and the electroweak mixing parameter to compare with the experimental measurement of A_{LR} , effectively including higher-order corrections in $\sin^2 \theta_W^{\text{eff}}$ (as well as a_e and v_e). This effective electroweak mixing parameter is then defined by

$$\sin^2 \theta_W^{\text{eff}} \equiv (1 - v_e/a_e)/4 \quad (3)$$

This convention is particularly useful for the measurement of the electroweak asymmetries at the Z resonance.

The A_{LR} event selection is very simple and is designed to efficiently select a pure sample of hadronic Z decays. Tau-pair and muon-pair final states are not explicitly excluded in the selection, but the efficiency is small. Bhabha events (e^+e^- final states) are excluded due to the complications involved in identifying and interpreting the large t -channel contribution. In the LAC we require $E_{tot} \equiv \sum E_i > 15$ GeV and $E_{imb} \equiv |\sum E_i \hat{r}_i|/E_{tot} < 0.6$, where the sums are over LAC clusters i having energy greater than 100 MeV and \hat{r}_i is a unit displacement vector from the collision point to the i th LAC

cluster. The only other criteria requires a few good tracks in the drift chamber: at least 3 tracks in one hemisphere or at least 2 tracks in both hemispheres. These criteria eliminate Bhabha, radiative Bhabha, 2-photon, and beam background events, resulting in a sample purity of $99.89 \pm 0.08\%$ with a selection efficiency of $89.3 \pm 0.8\%$.

The A_{LR} error is statistics dominated. By far the leading systematic error is that of the polarization measurement. Table 2. summarizes the polarization measurement errors for each SLC/SLD run. The entry labelled ‘‘AP’’ refers to the polarimeter analyzing power, that is, the expected Compton cross-section asymmetry for a fully-polarized beam. The kinematic cutoff for Compton scattering corresponds to electrons fully backscattered in the c.o.m. frame, which is also where the asymmetry is maximum. This provides a natural means for calibrating the polarimeter to the physical scale. The entry labelled ‘‘chromaticity’’ refers to a small effect which, due to imperfect beam chromatic corrections, allow the polarization at the e^+e^- IP to be slightly different than that measured at the $e^-\gamma$ IP some 25m away. Before the 1994-95 run a number of steps were taken to make this effect small, including changes to the electron-beam bunch compression and better and more frequent measurements of beam dispersion. For the 1996 run a second polarimeter (PGC) was installed to crosscheck the Compton polarization measurement at the $\sim 1\%$ level by measuring the Compton photon energy asymmetry, rather than the Compton electron asymmetry as with the standard polarimeter. Preliminary results show that the measurements agree to better than 1%.

Table 2: Systematic uncertainties on the polarization measurement, $\delta\mathcal{P}_e/\mathcal{P}_e$. The uncertainty for the 1996 run given below is inflated due to the preliminary nature of the analysis at the time of presentation. Subsequent analysis indicates a final error which again will be $\approx 0.7\%$.

	1992	1993	1994-95	1996
Laser Polarization	2.0%	1.0%	0.20%	0.20%
Detector Linearity	1.5%	1.0%	0.50%	0.50%
AP Calibration	0.4%	0.5%	0.29%	0.30%
Electronic Noise	0.4%	0.2%	0.20%	0.20%
Inter-channel consistency	0.9%	0.5%	—	0.8%
Total Polarimeter Uncertainty	2.7%	1.6%	0.67%	1.03%
Chromaticity (ξ)	—	1.1%	0.17%	0.18%
Total \mathcal{P}_e Uncertainty	2.7%	1.9%	0.69%	1.04%

2.1 Results

A complete expression which summarizes the A_{LR} measurement is

$$\begin{aligned}
A_{LR} = & \frac{A_m}{\langle\mathcal{P}_e\rangle} + \frac{1}{\langle\mathcal{P}_e\rangle} \{f_b(A_m - A_{\text{bkg}}) - A_{\mathcal{L}} + A_m^2 A_{\mathcal{P}} \\
& - E \frac{\sigma'(E)}{\sigma(E)} A_E - A_{\varepsilon} + \langle\mathcal{P}_e\rangle \mathcal{P}_p\}
\end{aligned} \tag{4}$$

The quantity A_m is the measured asymmetry in terms of numbers of events: $A_m = (N_L - N_R)/(N_L + N_R)$. The terms within the curly brackets represent very small, nearly negligible, corrections. The larger of these terms, the background correction (f_b), luminosity asymmetry ($A_{\mathcal{L}}$), and polarization asymmetry ($A_{\mathcal{P}}$), are summarized in Table 2.1. Note that all quantities are given in units of 10^{-4} . The individual polarization measurements \mathcal{P}_i associated with each Z^0 event are combined to form the luminosity-weighted average polarization:

$$\langle \mathcal{P}_e \rangle = (1 + \xi) \frac{1}{N_Z} \sum_i^{N_Z} \mathcal{P}_i, \quad (5)$$

where ξ is the chromatic correction discussed above. Table 2.1 summarizes the A_{LR} measurements [2, 3, 4] for each SLC/SLD run, and a complete description of all terms can be found in the references.

Table 3: Terms from Eq. 4 in units of 10^{-4} . The terms not shown are considered negligible. The corrections actually applied to A_m are given in the bottom row. The 1996 results are preliminary.

Quantity	1992	1994	1994-95	1996
A_m	223 ± 99	1031 ± 46	1144 ± 32	1178 ± 44
$f_b(A_m - A_{\text{bkg}})$	4.7 ± 1.6	1.75 ± 0.72	0.65 ± 0.55	0.65 ± 0.55
$A_{\mathcal{L}}$	1.8 ± 4.2	0.38 ± 0.50	-1.9 ± 0.3	0.0 ± 0.5
$A_m^2 A_{\mathcal{P}}$	—	-0.35 ± 0.01	0.31 ± 0.13	0.10 ± 0.13
A_m Correction	0.0 ± 4.5	1.0 ± 0.8	2.75 ± 0.79	0.76 ± 0.75

Table 4: Summary of SLD A_{LR} results. Analysis of the 1996 run is still in progress.

Run	Z Events	$\langle \mathcal{P}_e \rangle$ (%)	\sqrt{s} (GeV)	A_{LR}	Reference
1992	10.2×10^3	22.4 ± 0.7	91.55	$0.100 \pm 0.044 \pm 0.004$	PRL 70, 2515
1993	49.4×10^3	62.6 ± 1.1	91.26	$0.1628 \pm 0.0071 \pm 0.0028$	PRL 73, 25
1994-5	93.6×10^3	77.2 ± 0.5	91.28	$0.1512 \pm 0.0042 \pm 0.0011$	PRL 78, 2075
1996	51.4×10^3	76.5 ± 0.8	91.26	$0.1541 \pm 0.0057 \pm 0.0016$	preliminary

Each run has been carried out at slightly different center-of-mass energies. To be comparable to other measurements and to extract $\sin^2 \theta_W^{\text{eff}}$, the A_{LR} measurement must be corrected to the Z-pole. Hence, combining the above measurements and correcting to the Z-pole, including the small γ -Z interference correction, results in the cumulative result:

$$A_{LR}^0 = 0.1550 \pm 0.0034 \quad (6)$$

The corresponding value of $\sin^2 \theta_W^{\text{eff}}$, assuming the SM relationship of Eq. 2, is $\sin^2 \theta_W^{\text{eff}} = 0.23051 \pm 0.00043$. Finally, one can include the other less precise SLD lepton measurements of $\sin^2 \theta_W^{\text{eff}}$ due to the angular distributions of electron, muon, and tau-pair events,

as well as the so-called Q_{LR} measurement[5]. The combined result, still preliminary due to the 1996 results, is

$$\sin^2 \theta_W^{\text{eff}} = 0.23055 \pm 0.00041 . \quad (7)$$

2.1.1 LEP Comparison and Global Fits

One way to compare the SLD A_{LR} measurement of $\sin^2 \theta_W^{\text{eff}}$ with those from LEP is shown in Fig. 2.1.1. The two most precise measurements based on lepton couplings, A_{LR} and A_{FB}^ℓ (the lepton forward-backward asymmetry from LEP), agree at the 0.2σ level. On the other hand the combined lepton-based measurements disagree with the quark-based measurement (dominated by A_{FB}^b , the b -quark forward-backward asymmetry from LEP) by 2.7σ . It is interesting to speculate on whether the discrepancy represents a somewhat unlikely, but surely plausible, distribution of values about a central mean, or whether there is an experimental problem, or perhaps it is a hint of new physics.

As stated earlier, A_{LR} is substantially a rather simple event counting measurement. The one outstanding systematic is the scale of the beam polarization. From Table 2. one finds that the average error on the polarization scale is 1.0%, and this scale has been independently cross-checked many times at the 1–3% level. On the other hand, to force the A_{LR} measurement into agreement with the quark-based average of Fig. 2.1.1 would require a 9% uncertainty on the polarization scale. This is evidently not plausible. Clearly, if the discrepancy between leptons and quarks were to become more significant, then the implication would be for a non-SM explanation.

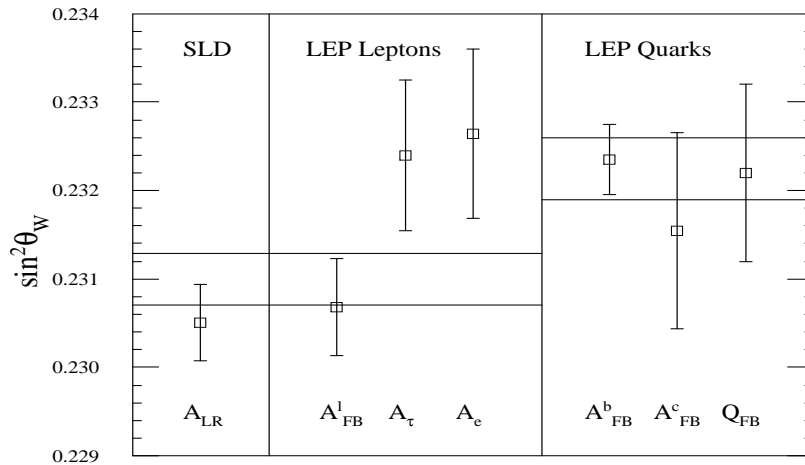


Figure 2: Comparison of Z^0 measurements of $\sin^2 \theta_W^{\text{eff}}$ for different techniques. The LEP results are from Moriond 1997. The horizontal bands represent the combined errors.

We have performed some global fits of the electroweak data, involving the fit of 5 parameters (m_t , M_H , α_s , $\alpha(M_Z^2)$, M_Z) to 19 observables. First of all, one can see how

well the precision measurements predict the top mass. The result is 155_{-9}^{+11} GeV/ c^2 , which is about 1.7σ from the measured value. This is not excellent agreement, but is probably acceptable. If the measured m_t is incorporated into the fit, one can derive a Higgs mass. The errors on the central value are still huge, implying that it should not be taken too seriously. However, the upper limit of $M_H < 419$ GeV/ c^2 at 95% CL is probably sufficiently well determined as to be meaningful.

The S - T framework[6] provides a more general tool for SM tests. Figure 2.1.1 indicates how several of the key measurements translate into bands of different slope in the S - T plane. Also shown are the SM predictions (crosses) centered on the origin, with T increasing with top mass (175 ± 6 GeV/ c^2) and M_H variation along the diagonal lines (1000 GeV/ c^2 lower right to 70 GeV/ c^2 upper left). There is generally good agreement between the data and the SM, although it is interesting to note that there is a hint of a second solution for the data at negative S and T .

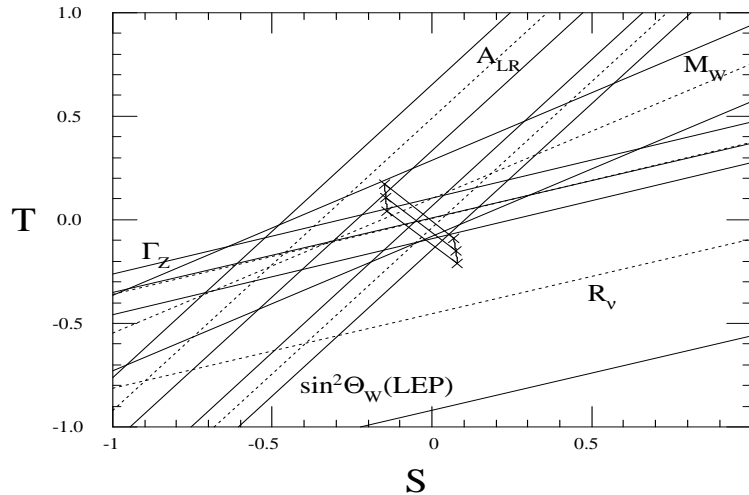


Figure 3: Analysis of global results using the S-T framework. Central values for the measurement bands are the dotted lines. The SM region is given by the central region bounded by crosses (see text).

3. The Z - b - \bar{b} Vertex

The process $Z^0 \rightarrow b\bar{b}$ has a set of unique vertex corrections involving the top quark and, potentially, physics beyond the SM, which are quite different from the oblique corrections which modify the theoretical value of $\sin^2 \theta_W^{\text{eff}}$. For example, in addition to vertex correction diagrams involving t - b - W^\pm couplings, one can also have t - b - H^\pm . The primary observables used to describe this physics are the fraction of hadronic Z^0 decays which are to $b\bar{b}$, $R_b = \Gamma_b/\Gamma_{\text{had}}$, and the b -quark parity violation parameter A_b . To lowest order, the SM expressions for these quantities in terms of the axial-vector and vector

couplings, or the left and right-hand couplings, of the b -quark to the Z^0 are given by

$$R_b \propto v_b^2 + a_b^2 \propto g_L^2 + g_R^2; \quad A_b = \frac{2a_e v_2}{a_e^2 + v_e^2} = \frac{g_L^2 - g_R^2}{g_L^2 + g_R^2} \quad (8)$$

With $g_L = -0.42$ and $g_R = 0.08$ we see that R_b and A_b are quite complimentary: R_b is 5.5 times more sensitive to g_L than g_R , whereas A_b is 5.5 times more sensitive to g_R than g_L .

3.0.2 Topological Vertexing and VXD3 Results

The vertexing resolution available with SLD allows one to exploit qualitatively new analysis techniques. The intrinsic resolution of VXD3 demonstrated with 1996 data is $4.7 \mu\text{m}$ in r - ϕ and $4.5 \mu\text{m}$ in z . Topological vertexing refers to the reconstruction of displaced vertices and the tracks which emanate from them. The tracks can then be combined and their properties compared to Monte Carlo. In particular, the invariant mass of the tracks is a very powerful discriminant of bottom mesons relative to charm. In fact, the kinematic information available can be used to partially compensate for unmeasured (neutral) decay products. If M_{raw} is the mass from the measured mass, the corrected mass is given by $M = \sqrt{M_{\text{raw}}^2 + p_T^2} + p_T$, where p_T is the transverse momentum of the visible tracks relative to the axis formed by the line from primary collision point to reconstructed decay vertex. The resulting mass distribution is given in Fig. 3.0.2, and is compared to Monte Carlo, where one can see a clear separation between bottom and charm (as well as light quarks). This particular distribution is for 1996 data with VXD3. This separation is key for eliminating charm contamination and systematics which have plagued b -quark measurements, in particular the R_b measurement described below.

3.1 Direct A_b and A_c Measurements

The differential cross section for b -quark production with polarized beam is

$$\frac{d\sigma}{d\cos\theta} \propto (1 - \mathcal{P}_e A_e) (1 + \cos^2\theta) + 2\cos\theta (A_e - \mathcal{P}_e) A_b \quad (9)$$

The beam polarization, \mathcal{P}_e , in this expression can be of either sign. There are two important aspects of the polarized angular asymmetries which are readily apparent from this expression. First, the A_b term is modulated by the product $\mathcal{P}_e A_b$. This is contrasted with the unpolarized forward-backward asymmetry for which the asymmetry term is modulated by the product $A_e A_b$. Hence, the SLD measurement represents a direct A_b measurement, rather than a product of two SM parameters. Secondly, the much larger polarized asymmetry implies a statistical advantage by a factor $(\mathcal{P}_e/A_e)^2 \approx 25$.

For this measurement vertexing is required only to identify $b\bar{b}$ final states, which is relatively straightforward. For previous measurements this was accomplished using a minimum number of tracks with a significant 2-D impact parameter relative to the primary collision point. This is now done using the SLD topological vertexing method,

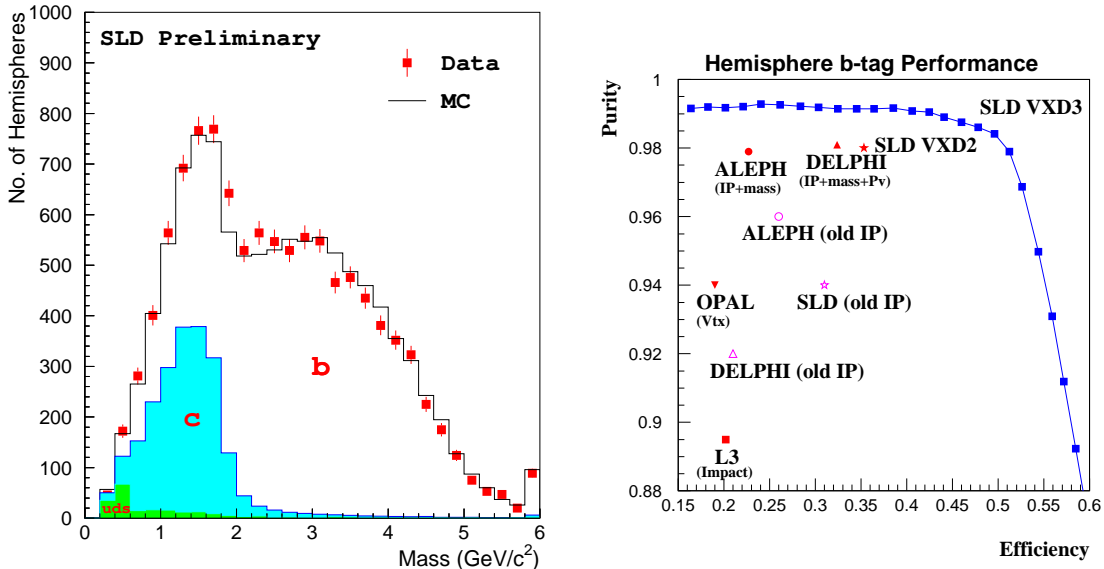


Figure 4: Left: Reconstructed mass of secondary vertex decay products using topological vertexing. The data points are for the 1996 run with VXD3. This agrees well with the MC, for which the expected contributions due to b , c , and u, d, s are indicated. Right: Hemisphere b -tag performance in efficiency-purity plane for SLD. Recent improvements in tagging techniques from LEP (except for DELPHI) are not yet included in the plot.

discussed in the preceding section. Once the event is tagged, it is necessary to identify which jet is the b -jet. This has been carried out in three analyses: using the jet charge technique, using the sign of the charge of a high- p_T lepton from semi-leptonic b or \bar{b} decays, or using the sign of charge of a K^\pm due to $b \rightarrow c \rightarrow s$ and identified by the CRID system. The lepton[8] and kaon analyses rely on Monte Carlo (MC) to determine the relative u, d, s, c , and b contributions as well as the probability of correctly assigning b and \bar{b} . On the other hand the jet charge technique[9] is self calibrating, with very little dependence on MC. The left-hand plot of Fig. 3.1 shows the distributions from the 1994–95 run to which Eq. 9 is fit to extract A_b . One clearly sees both large left-right and forward-backward asymmetries. The A_c measurement is performed analogously, where the final state involves either sign of lepton charge in semi-leptonic charm decays or sign of charge of reconstructed D or D^* mesons.

A compilation of SLD and LEP results for A_b and A_c is given in Fig. 3.1. The SLD kaon analysis has been updated since Winter 1996. As discussed above, since the LEP experiments measure the product $A_e A_b$ ($A_e A_c$), a value of A_e must be specified to extract A_b (A_c). For these plots the combined LEP-SLD value of $A_e = 0.1512 \pm 0.0023$ has been used. One sees that for A_b there is a substantial disagreement of 2.7σ between

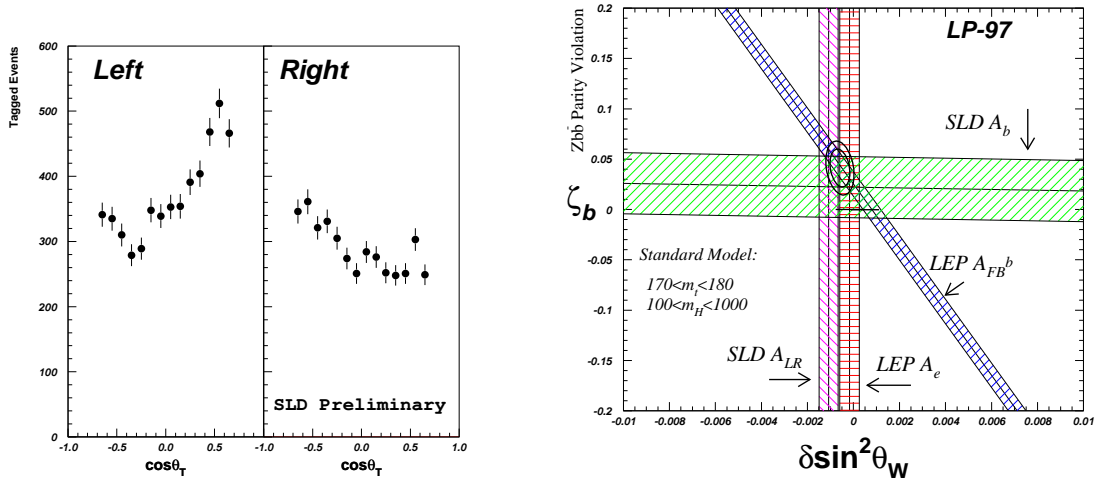


Figure 5: Left: Angular distributions for $Z \rightarrow b\bar{b}$, plotted separately for left and right-hand polarized electron beam. Right: Analysis of Ref. 7 applied to the LEP-SLD measurements of A_b and $\sin^2 \theta_W^{\text{eff}}$. The horizontal line centered at the origin represents the SM prediction for the ranges $170 < m_t < 180 \text{ GeV}/c^2$ and $100 < M_H < 1000 \text{ GeV}/c^2$, and using as input $\alpha_s = 0.117$ and $\alpha = 1/128.96$. The ellipses are the combined experimental 68% and 90% CL error contours.

the experimental average and the SM prediction. It is sometimes convenient to express deviations from the SM Z - b - \bar{b} couplings as a linear combination of left and right-handed terms. Specifically, the couplings ξ_b and ζ_b are chosen[7] such that R_b depends only on ξ_b and A_b only on ζ_b , and as such ζ_b is independent of m_t . The right-hand plot of Fig. 3.1 gives ζ_b vs $\sin^2 \theta_W^{\text{eff}}$ from LEP and SLD compared to the SM predictions, centered at the origin. The agreement of the SM to the combined experimental result is rather poor.

3.2 Measurement of R_b and R_c

A serious challenge to the R_b measurement has been the need to accurately determine the charm background. In SLD, topological vertexing combined with the mass selection of Fig. 3.0.2 has greatly reduced the charm contamination and hence obviated the reliance on troublesome MC charm modelling. SLD applies this b -tag separately to each event hemisphere, therefore measuring the rate of single tags and double tags. In this way, one determines directly from the data not only the b fraction, but also the b -tag efficiency. The right-hand plot of Fig. 3.0.2 shows the SLD (VXD3) contour for hemisphere b -tag measurement in the efficiency-purity plane.

SLD also uses the vertex double-tag technique for its R_c measurement, and is, so far,

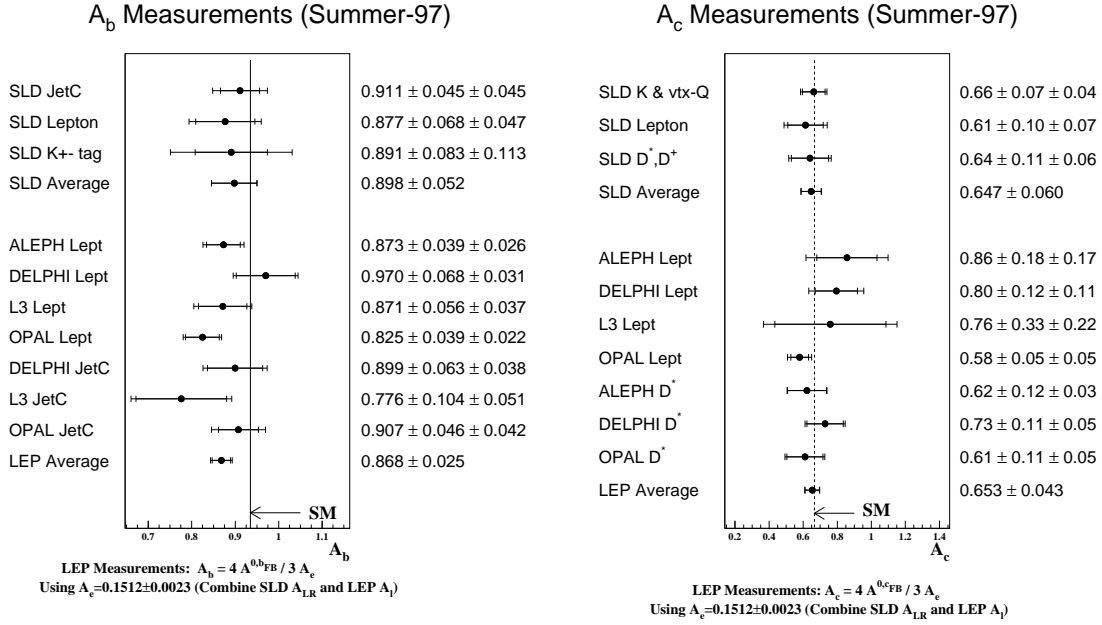


Figure 6: Comparison of world A_b (left) and A_c (right) measurements.

unique in doing so. The two major c -tag selection criteria are a vertex mass cut ($0.6 < M < 2.0 \text{ GeV}/c^2$) within the charm region of Fig. 3.0.2 and a cut on the momentum of the reconstructed decay vertex, which exploits the fact that for a given vertex mass, D mesons have a larger momentum than do B mesons. The resulting hemisphere c -tag efficiency and purity (with VXD3) are $14.0 \pm 1.3\%$ and $67 \pm 2\%$, respectively.

A compilation of SLD and LEP results for R_b and R_c is given in Fig. 7. The measurements from both SLD and LEP have improved substantially since 1995, when there was an apparent 3σ discrepancy in R_b between experiment and the SM. Reduction of charm background using vertex mass, as done by SLD and ALEPH, along with better treatment of hemisphere correlations by all groups, has improved the experimental result. And now the SM prediction lies within the 68% CL experimental error ellipse.

4. B Mixing

Measurement of $B^0-\bar{B}^0$ mixing provides an excellent means for testing the SM, especially the CKM sector and the SM description of CP violation. SLD and all LEP experiments have reported measurements of B_d^0 mixing, as outlined below. No measurement has yet been made of B_s^0 mixing, although there are limits from LEP. Because of the rapid oscillations expected in the B_s case, vertexing resolution is very important. In addition to its excellent vertexing, SLD also benefits greatly from polarized beam for initial-state tagging. Hence, if SLC can deliver good luminosity, then SLD will be well positioned to

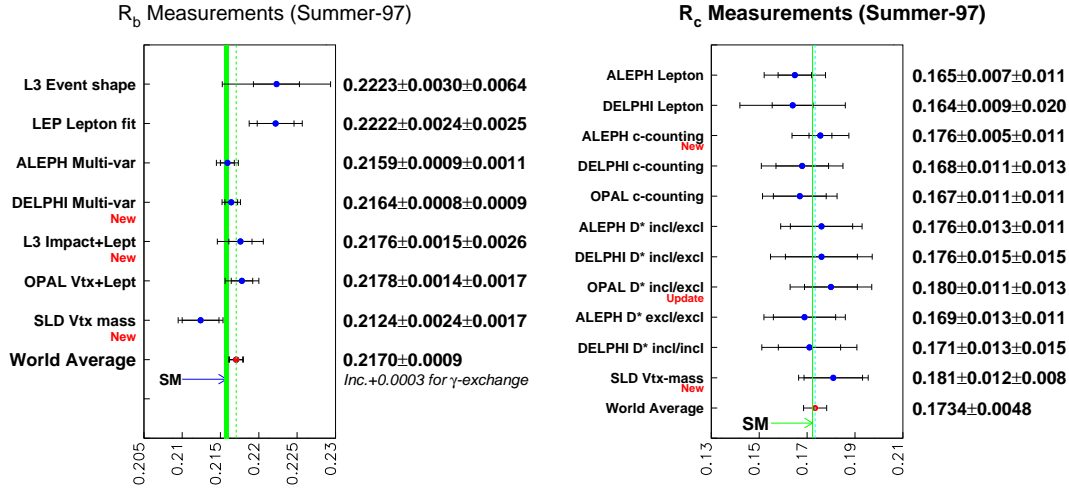


Figure 7: Comparison of world R_b (left) and R_c (right) measurements.

make this difficult measurement.

The considerable interest in making a B_s^0 mixing measurement derives largely from the following considerations. The mixing box diagrams give the following expression for the measureable ratio of mass eigenstate splitting for B_s relative to B_d :

$$\frac{\Delta m_s}{\Delta m_d} = \frac{\eta_s M_s f_s^2 B_s |V_{ts}|^2}{\eta_d M_d f_d^2 B_d |V_{td}|^2} = (1.32 \pm 0.09) \frac{M_s |V_{ts}|^2}{M_d |V_{td}|^2} \quad (10)$$

Here, η , M , f , and B represent, respectively, the QCD correction, the mass, the decay constant, and the degree to which the mixing occurs via box diagrams. The quantities f and B in particular are not well determined. However in ratio they are determined to $< 10\%$ from lattice calculations, as indicated by the numerical value given[10]. Since V_{ts} is derived from unitarity, the B_s mixing measurement will present a good measure of what is the most poorly known side of the unitarity triangle, V_{td} . Hence, the measurement will pinpoint the apex (ρ, η) of the unitarity triangle and, in fact, provide a substantial test of the SM picture of CP violation by checking that, in fact, such a triangle exists.

4.1 B_d Mixing Measurement

Once a sample of $Z \rightarrow b\bar{b}$ events has been identified, a mixing measurement involves three major requirements:

1. The proper time between the B^0 production at the collision point and the B^0 (or \bar{B}^0 if mixing has occurred) decay vertex. This is determined from the observed decay length and the measured boost.
2. An initial-state tag to determine B^0 vs \bar{B}^0 at production.
3. A final-state tag to determine if mixing has occurred by the time of decay.

The large forward-backward asymmetry for $Z \rightarrow b\bar{b}$ with polarized beam is measured to extract A_b , as described above. However, this asymmetry can now be exploited to tag the initial-state flavor of a b jet from its production angle. One can combine this with the jet-charge technique to produce an initial-state tag which is correct with a probability of $\approx 74\%$ for $\mathcal{P}_e = 77\%$. The final state tag is carried out using four different techniques in SLD. Two of these involve using semi-leptonic decay events, one using a reconstructed D meson and the other being more inclusive. The third uses the charge of a K^\pm as identified by the CRID system. This is similar to that used for the A_b analysis. Finally, there is a ‘‘charge dipole’’ tag, which uses 3-D topological vertexing to look for a charge separation (dipole) due to the $b \rightarrow c$ decays. The mixing signals for all four of these techniques are shown separately in Fig. 4.1.

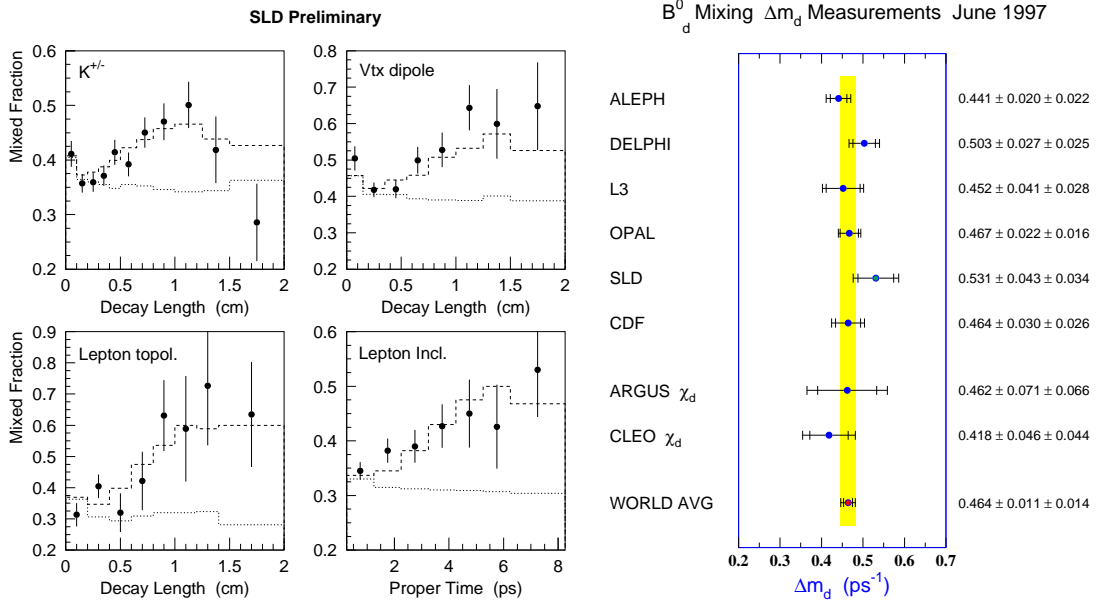


Figure 8: Left: SLD results for B_d^0 mixing for the four different analysis techniques used for final-state tagging. The dotted lines correspond to the MC result with no mixing, while the dashed line is the fitted mixing result. Right: Comparison of world B_d^0 mixing results.

4.1.1 B_s Mixing Prospects

The SLD analysis for B_s^0 mixing is similar to that described above for B_d^0 . Initial-state tagging is the same, and the final-state tag techniques are similar. The primary qualitative difference is the rapid oscillations, where the mixing parameter $x_s = \Delta m_s/\Gamma_s = 1.55 \Delta m_s$ is already known to be greater than about 14, implying many mixing oscillations within a decay lifetime. This puts a premium on vertex detector resolution. In particular, the “charge dipole” final-state tagging technique mentioned above actually doubles in statistical power relative to the B_d^0 case.

The estimate for the SLD reach with $\sim 500 \times 10^3$ Z^0 events (with VXD3), when expressed as a limit, is $\Delta m_s < 18 \text{ ps}^{-1}$ at 95% CL. This is significant, as it covers essentially the entire presently allowed region for the apex point (ρ, η) of the unitarity triangle. Hence, given enough luminosity, SLD would be guaranteed to see the mixing or place very interesting limits on it.

5. Summary and Prospects

The SLD A_{LR} measurement continues to be the single most precise measurement of $\sin^2 \theta_W^{\text{eff}}$, with the cumulative result being $\sin^2 \theta_W^{\text{eff}} = 0.23051 \pm 0.00043$. This agrees well with the cumulative LEP result derived from lepton couplings, but disagrees with the LEP quark-derived value of $\sin^2 \theta_W^{\text{eff}}$ at 3.1σ , and differs from the global LEP average by 2.8σ . The polarized forward-backward asymmetries allow direct measurement of A_b and A_c , which are mostly sensitive to the right-hand vertex couplings. The world data for A_b presently disagree with the SM at the 2.7σ level. The SLD measurement of R_b , after careful elimination of charm with precision vertex measurement and topological vertex reconstruction, is in good agreement with the SM.

The error on the measurement of A_{LR} is dominated by the event statistics, N_Z , and this will continue into the future. To excellent approximation the error on $\sin^2 \theta_W^{\text{eff}}$ from A_{LR} is

$$\delta \sin^2 \theta_W^{\text{eff}} = \frac{1}{7.9} \left[\frac{1}{N_Z \mathcal{P}_e^2} + A_{LR}^2 \left(\frac{\delta \mathcal{P}_e}{\mathcal{P}_e} \right)^2 \right]^{1/2}, \quad (11)$$

where \mathcal{P}_e is the electron-beam polarization measurement, which is the dominant systematic error. Hence, one can extrapolate the error with much confidence. The other key measurements can also be extrapolated for more data. This is summarized below in Table 5.. The most difficult to extrapolate is that for B_s^0 mixing. Since some of these measurements, especially A_{LR} and A_b are currently in marginal disagreement with the Standard Model, it is certainly of great interest to improve the errors and determine if there really is, or is not, an indication of physics beyond the Standard Model. In addition, SLD has unique sensitivity to B_s mixing, for which the measurement would make a substantial test of the SM model of CP violation.

Table 5: Current errors for a few key electroweak observables for LEP and SLD now, and estimates for SLD near future (1998) and assuming additional running.

Quantity	LEP 1996 (combined)	SLD 1996	SLD 1997-98 ($\sim 150\text{k Zs}$)	SLD+ 350k more Zs
$\sin^2 \theta_W^{eff}$	± 0.00027	± 0.00041	± 0.00029	± 0.00021
A_b	± 0.025	± 0.040	± 0.032	± 0.023
R_b	± 0.0012	± 0.0027	± 0.0020	± 0.0014
Δm_s (ps^{-1}) (95% CL)	8–10	in progress	12	18

References

- [1] M. Woods, AIP Conference Proc. 343, 230 (1995).
- [2] SLD Collab., Phys. Rev. Lett. 70, 2515 (1993).
- [3] SLD Collab., Phys. Rev. Lett. 73, 25 (1994).
- [4] SLD Collab., Phys. Rev. Lett. 78, 2075 (1997).
- [5] SLD Collab., Phys. Rev. Lett. 78, 17 (1997).
- [6] T. Takeuchi and M. Peskin, Phys. Rev. D46, 381 (1992).
- [7] T. Takeuchi, A.K. Grant, and J.L. Rosner, Proc. DPF94, 1231 (1994), hep-ph/9409211.
- [8] SLD Collab., Phys. Rev. Lett. 74, 2895 (1995).
- [9] SLD Collab., Phys. Rev. Lett. 74, 2890 (1995).
- [10] A. Abada, *et al.*, Nucl. Phys. B376, 172 (1992);
A. Soni, Brookhaven preprint BNL-61378 (1995).